Kinematics of a 4-DoF Series-Parallel Robotic Thumb

Nicholas Baiata[1] and Nilanjan Chakraborty[1]

***Abstract*— Series-parallel robotic fingers offer a slender form factor, with excellent force transmission and potential controllability. A challenge in designing robotic hands with series-parallel fingers is that the fingertip position is hard to control because it is difficult to analyze the finger kinematics for fingers with 3–Degree-of-Freedom (3-DoF) or higher. In previous work [1], we have partially overcome this challenge by designing and analyzing a 3-DoF series-parallel finger. However, the thumb is a special finger, which needs at least 4-DoF for it to be part of a versatile hand with the ability to do both opposable-thumb grasping as well as open-palm manipulation. The only current series-parallel hybrid hand available (AIDIN) has a fixed position thumb (3-DoF), resulting in the loss of open-palm manipulation, and a reduction in dexterity and manipulable object size. Therefore, in this paper, we present the kinematic design and analysis of a novel 4-Degree-of-Freedom (4 DoF) series-parallel hybrid robotic thumb. We present the forward, inverse, and differential kinematics, and show via simulation that we can do position control and velocity control of the thumb in the joint space as well as the task space. A video of the MATLAB Simulink simulations can be found at `https://youtu.be/qrf0sRCv0kQ`.**

I. INTRODUCTION

The availability of a compact and versatile robotic hand capable of opposable thumb as well as open-palm manipulation is key for developing robots with dexterous manipulation capabilities to help in a wide variety of applications ranging from industrial operations to assistive robotics in homes. Consequently, a wide variety of robotic hands, many of which are optimized towards applications like pick-and-place, have been proposed [2], [3]. These hands can be classified into hands with rigid fingers or soft fingers. Further, key types of rigid fingers proposed are direct-drive, tendon-driven, and linkage-driven [4]. While underactuated hands (hands with soft fingers as well as some tendon-driven hands) are great for power grasping, it is hard to use them for dexterous manipulation because of the difficulty of fingertip positioning and force control [5].

Direct-drive hands are the easiest to control, but they are inherently limited by their motor placement [6]. Larger motors equate to more grasping force, but also larger fingers and less dexterity. Smaller motors grant more dexterity, at the cost of grasping force. Tendon-driven hands solve this issue by moving the motors to the forearm, and actuating the joints via stretchable tendons, such as in the Shadow Robot Dexterous Hand [7]. This results in a very slender hand. However, one cannot push a tendon, so two motors are needed for each degree of freedom. This introduces additional weight, costs, and size (in the forearm). The non-rigid body tendons also introduce more complicated dynamics and hence, control schemes. Linkage-driven hands offer a medium: put the motors in the palm, and actuate the finger with rigid links. This gives slender fingers, with good force output, and one motor per degree of freedom; however, the kinematic analysis and hence the control becomes challenging for fingers with 3–Degree-of-Freedom (3–DoF) or higher [6].

This work was partially supported by the US Department of Defense through ALSRP under award No. HT94252410098, a SBU OVPR award, and a SBU LINCATS award. Nicholas Baiata was supported by a Department of Education GAANN fellowship.

[1]The authors are with the Department of Mechanical Engineering at Stony Brook University, NY, USA. Email: {nicholas.baiata, nilanjan.chakraborty}@stonybrook.edu.

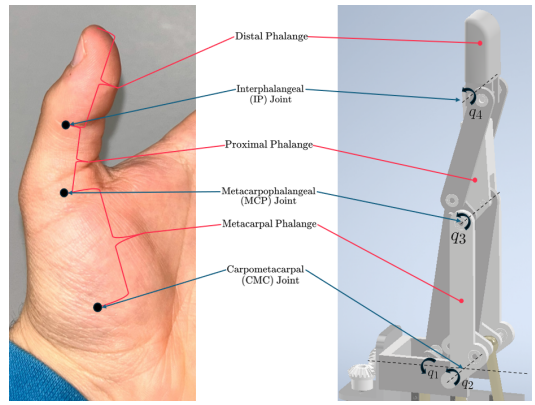

Fig. 1. Anatomic comparison of human thumb and the proposed 4-DoF series-parallel thumb mechanism

The only commercially available linkage-driven robotic hand is the AIDIN hand [6], [8], which employs a three-dimensional parallel linkage chain at the base of the fingers, and as such no forward or differential kinematics have been presented by the authors. Zaw et al. were able to achieve the same range of motion while collapsing the parallel linkage chain down to two dimensions, and successfully presenting the forward, inverse, and differential kinematics [1]. Thus, we could obtain the finger Jacobian, which is crucial for force analysis/control as well as motion planning in the task space [9]. Additionally, the AIDIN hand makes no special distinction for the thumb; instead, it is simply another 3-DoF finger locked in an opposed position relative to the other four fingers (i.e., opposable thumb configuration). This reduces the ability of the hand to manipulate larger objects and limits the amount of force the hand can output during a power-push (because the finger tips have to be used for pushing instead of the whole palm).

Although the human thumb has 5-DoF [10], we can approximate its range of motion using a 4-DoF mechanism [11]. Therefore, in this paper, we tackle the problem of designing a 4-DoF thumb that can switch between opposable thumb configuration and open palm configuration. The *key contribution of this paper is to extend the work in [1] to present a novel 4–DoF series parallel thumb, and present*

solutions for the forward, inverse, and differential kinematics of this thumb. This allows us to design position/velocity control schemes for the tip of the thumb, which could serve as a building block for creating compact hands with dexterous manipulation capability. We present simulation results showing the capability of fingertip control.

II. Overview of Thumb Design

We will first briefly describe some terminology and naming conventions of hand bones and joints that will be used throughout the paper. Abduction/adduction refers to side-to-side movement (commonly referred to as finger *wagging*), while flexion/extension describes the bending and unbending motions. For brevity, the terms "abduction/adduction" and "flexion/extension" will be referred to as "abduction" and "flexion," respectively. At the base, we have the carpometacarpal (CMC) joints. The CMC joints of the fingers are more associated with wrist movements and are typically not considered in robotic finger designs. However, the CMC joint of the thumb plays a critical role in both abduction and flexion motions. The metacarpals connect the CMC joint to the metacarpophalangeal (MCP) joint, which also provides both abduction and flexion. The proximal phalanx connects the MCP joint to the interphalangeal (IP) joint. The IP joint only allows for flexion, and connects to the distal phalanx (also known as the *thumbtip*) [10].

The term "series-parallel hybrid" comes from the mechanical design, which features six closed-loop linkages, each described by some loop closure equation. Within these loops there are "serial" joint angles, q_1, q_2, q_3, and q_4, and "intermediate" joint angles, β_1, β_2, and β_3. The serial joint angles correspond to the actual joint motions of the thumb, where q_1 is the abduction of the CMC joint, and q_2, q_3, and q_4 is the flexion of the CMC, MCP, and IP joints, respectively (see Figure 1). The serial links connect these joints, and correspond to the actual bones in the human thumb. The intermediate angles correspond to the angles of the bellcranks which translate motion from the motors to the serial joints.

Figure 2 shows the bellcranks and other intermediate links in gray, and the serial links in dark blue. The "abductor", in light blue, rotates according to q_1 (abduction motion). Since this joint is located in the palm, it is simply driven via direct drive. This results in a thicker palm, specifically the backside of the palm, but the finger dimensions remain unaffected. The other motors, M_2, M_3, M_4 are linear actuators, and can be seen in Figure 2 in orange, pink, and green, respectively. Because the abduction motion is orthogonal to the flexion motion, the linkages connecting the linear actuators to the bellcranks and serial links must have spherical joints on both ends. These links are commonly described as Prismatic-Spherical-Spherical (PSS) chains. Using appropriate link lengths we were able to achieve a range of motion of 0°–90°for the flexion of the CMC, MCP, and IP joints, as well as ±40°for the abduction of the CMC joint. The force output of the thumb is dependent on the link lengths, which must be designed with the entire hand in mind in order to ensure ample workspace overlap for pinching tasks. As such, it will not be discussed in this paper as we aim to simply portray the kinematics of the thumb.

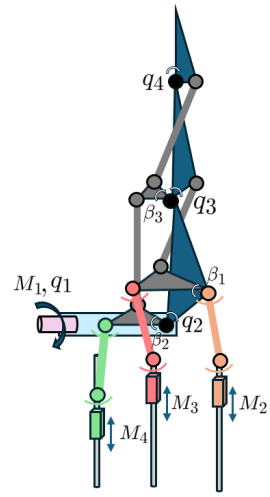

Fig. 2. Simplified Kinematic Model

III. Kinematic Analysis Methods

A. Forward Kinematics

When solving the forward kinematics of a mechanism, our goal is to relate the motor inputs to the end-effector pose. In a direct drive mechanism, each motor input can be directly mapped to a single joint angle. As such, the forward kinematics are typically expressed as the relationship between the joint angles and the end-effector pose. This simplification cannot be made for our mechanism, which uses bellcranks to transmit motion from the motors to the serial joints. The transmission of this motion can be described using loop closure equations. By systematically solving these equations, starting with the motor inputs, we can find the intermediate and serial joint angles, then construct homogeneous transformation matrices to directly relate the serial joint angles to the end effector position.

M_2, M_3, and M_4 can be used to find q_2, β_1, and β_2, respectively. From there, q_2 and β_1 can be used to find q_3, and q_2 and β_2 can be used to find β_3. Finally q_3 and β_3 can be used to find q_4. Figure 3 shows one such loop, which relates M_4 to β_2. The displacement of the carriage (M_4) from the reference frame $\mathcal{J}_{\beta_2}$, is denoted $\mathbf{U}_4$. The length of the PSS chain, l_4, is a scalar. The unknown rotation is the angle of the second bellcrank, β_2, which is embedded into the rotation matrix $\mathbf{R}_4$, which rotates the vector along the bellcrank, $\mathbf{V}_4$. By definition of the loop closure equations we know the magnitude of $\mathbf{U}_4$ and the unknown rotation, $\mathbf{R}_4\mathbf{V}_4$, must be equal to the magnitude of l_4, i.e.

$$\mathbf{U}_4^T\mathbf{R}_4\mathbf{V}_4 = \frac{\|\mathbf{U}_4\|^2 + \|\mathbf{V}_4\|^2 - l_4^2}{2} \tag{1}$$

Multiplying out the left-hand side will yield a long polynomial, which can then be simplified into the following form:

$$\mathrm{A}_4 \sin(\beta_2) + \mathrm{B}_4 \cos(\beta_2) + \mathrm{C}_4 = 0 \tag{2}$$

where C_4 includes the right-hand side of Equation 1, along with any other constants resulting from the multiplication of the left-hand side. The solution to this equation is a known trigonometric problem [12].

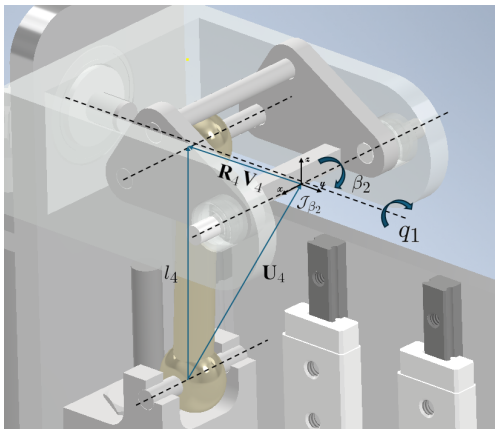

Fig. 3. M_4 to β_2 Loop

After finding all the serial angles, the transformation from the world frame $\mathcal{O}$ (located at the MCP joint) to the end-effector frame $\mathcal{J}_{EE}$ (located at the end of the distal phalanx) can be represented by the homogeneous transformation $T_{\mathcal{O}}^{\mathcal{J}_{EE}}$,

$$T_{\mathcal{O}}^{\mathcal{J}_{EE}} = T_{\mathcal{O}}^{\mathcal{J}_1} T_{\mathcal{J}_1}^{\mathcal{J}_2} T_{\mathcal{J}_2}^{\mathcal{J}_3} T_{\mathcal{J}_3}^{\mathcal{J}_4} T_{\mathcal{J}_4}^{\mathcal{J}_{EE}} \tag{3}$$

where $T_{\mathcal{O}}^{\mathcal{J}_1} = \mathbf{T}(\mathbf{R}_y(q_1), 0)$, $T_{\mathcal{J}_1}^{\mathcal{J}_2} = \mathbf{T}(\mathbf{R}_z(q_2), 0)$, $T_{\mathcal{J}_2}^{\mathcal{J}_3} = \mathbf{T}(\mathbf{R}_z(q_3), \mathbf{d}_1)$, $T_{\mathcal{J}_3}^{\mathcal{J}_4} = \mathbf{T}(\mathbf{R}_z(q_4), \mathbf{d}_2)$, $T_{\mathcal{J}_4}^{\mathcal{J}_{EE}} = \mathbf{T}(0, \mathbf{d}_3)$, and $\mathbf{d}_1$, $\mathbf{d}_2$,and $\mathbf{d}_3$ are the distances between the CMC joint and MCP joint, MCP joint and IP joint, and the length of the distal phalanx, respectively. Here $\mathbf{R}_n(q)$ is a pure rotation about the n-axis by angle q, $n \in \{x, y, z\}$, $\mathbf{R}_n(q) \in$ SO(3), and $\mathbf{T}(\mathbf{R}_n(q), \mathbf{d})$ is a homogeneous transformation with rotation $\mathbf{R}_n(q)$ and translation $\mathbf{d} \in \mathbb{R}^3$.

B. Inverse Kinematics

For a given end-effector location, **EE** (EE_x,EE_y,EE_z), we can first solve for the serial joint angles using traditional inverse kinematics. Then, using the loop closure equations, we can solve for the intermediate joint angles, and finally the motor positions. Since all translation along the x-axis is due to the abduction motion, q_1 can be found using

$$q_1 = \arctan2(\mathrm{EE_x}, \mathrm{EE_z}) \tag{4}$$

After q_1 is found **EE** can be 'un-rotated' by angle $-q_1$ in order to simplify the problem to the 3-R planar case, which has well documented solutions [9]. With all the serial angles, we can use the loop closure equations exactly as described in section III-A to find the intermediate joint angles. We can also use the loop closure equations to solve for the motor positions, though this time the unknown is not affected by a rotation, making the solution even simpler [6].

C. Differential Kinematics

The standard Jacobian is represented with: $\mathbf{J} = [\mathbf{J}_v, \mathbf{J}_\omega]^T$ where $\mathbf{J}_v$ is the linear velocity Jacobian, and $\mathbf{J}_\omega$ is the angular velocity Jacobian. These can be constructed separately, then concatenated. Typically each column in the linear velocity Jacobian would be represented by $[\frac{\partial x}{\partial q_i}, \frac{\partial y}{\partial q_i}, \frac{\partial z}{\partial q_i}]^T$, however, we are controlling the motors, not the joints, so we need $[\frac{\partial x}{\partial \mathrm{M}_i}, \frac{\partial y}{\partial \mathrm{M}_i}, \frac{\partial z}{\partial \mathrm{M}_i}]^T$, for i=1,2,3,4. This can be done by extracting the first three rows from the last column of $\frac{\partial T_{\mathcal{O}}^{\mathcal{J}_{EE}}}{\partial \mathrm{M}_i}$, where:

$$\frac{\partial T_{\mathcal{O}}^{\mathcal{J}_{EE}}}{\partial \mathrm{M}_i} = \sum_{j=1}^{4} \frac{\partial T_{\mathcal{O}}^{\mathcal{J}_{EE}}}{\partial q_j} \frac{\partial q_j}{\partial \mathrm{M}_i} \tag{5}$$

Each transformation matrix in Equation 3 has, at most, one serial joint angle. We must simply take the derivative of each and apply the chain rule accordingly in order to find $\frac{\partial T_{\mathcal{O}}^{\mathcal{J}_{EE}}}{\partial q_j}$. Finding all the joint-motor relationships, $\frac{\partial q_j}{\partial \mathrm{M}_i}$, is not as straightforward. A key simplification to realize is that not all motors effect all joints, i.e. M_4 only effects the distal phalanx, therefor $\frac{\partial q_3}{\partial \mathrm{M}_4} = \frac{\partial q_2}{\partial \mathrm{M}_4} = \frac{\partial q_1}{\partial \mathrm{M}_4} = 0$. Let's look at how you could treat one of the loops to find the joint/motor relationships. Loop 1 contains the variables q_1, q_2, and M_2. We can represent the partial derivative of the loop closure equation with respect to q_1 as A, q_2 as B, and M_2 as C. We can now relate q_2 to M_i for i = 1, 2

$$0 = \mathrm{A}\frac{\partial q_1}{\partial \mathrm{M}_i} + \mathrm{B}\frac{\partial q_2}{\partial \mathrm{M}_i} + \mathrm{C}\frac{\partial \mathrm{M}_2}{\partial \mathrm{M}_i} \tag{6}$$

$\frac{\partial \mathrm{M}_2}{\partial \mathrm{M}_1} = \frac{\partial q_1}{\partial \mathrm{M}_2} = 0$, resulting in:

$$\frac{\partial q_2}{\partial \mathrm{M}_1} = -\frac{\mathrm{A}}{\mathrm{B}}\frac{\partial q_1}{\partial \mathrm{M}_1} \tag{7}$$

$$\frac{\partial q_2}{\partial \mathrm{M}_2} = -\frac{\mathrm{C}}{\mathrm{B}} \tag{8}$$

The columns of $\mathbf{J}_\omega$ are typically the various joints' axis of rotation in the world frame. However, once again, we must adjust the Jacobian as we are multiplying it by the motor velocities, not the joint velocities. We can do this by multiplying each component of the angular velocity Jacobian by the appropriate vector of previously derived joint-motor relationships.

$$J_\omega = \sum_{n=1}^{4} \mathbf{R}_{\mathcal{O}}^{\mathcal{J}_n} \hat{\boldsymbol{\omega}}_n \begin{bmatrix} \frac{\partial q_n}{\partial M_1} & \frac{\partial q_n}{\partial M_2} & \frac{\partial q_n}{\partial M_3} & \frac{\partial q_n}{\partial M_4} \end{bmatrix} \tag{9}$$

where $\mathbf{R}_{\mathcal{O}}^{\mathcal{J}_n}$ is the rotation matrix from the base frame to the frame at joint *n*, i.e. $\mathbf{T}_{\mathcal{O}}^{\mathcal{J}_n}$(1:3,1:3) and $\hat{\boldsymbol{\omega}}_n$ is the axis of rotation at the nth joint. The full derivation of the forward, inverse, and differential kinematics can be found in [11].

IV. Kinematic Simulations

All simulations were conducted using MATLAB Simulink with resolved rate motion control [13]. Equation 10 describes the relationship between the end effector velocity ($d\mathbf{X}$) and the corresponding motor velocities ($d\mathbf{M}$).

$$d\mathbf{M} = \mathbf{J}^{-1} d\mathbf{X} \tag{10}$$

Using the pseudo-inverse of the Jacobian derived in section III-C, and given input velocity, we can command the thumb tip to move to a given pose within an error threshold. For the simulations here, we used 0.25 mm in each Cartesian direction, and 1° for the distal phalanx (thumb tip) angle, α, as our error threshold. Each case demonstrates a unique type of movement, with accompanying figures that shows the goal path, the path returned by the Simulink 'transform' sensor,

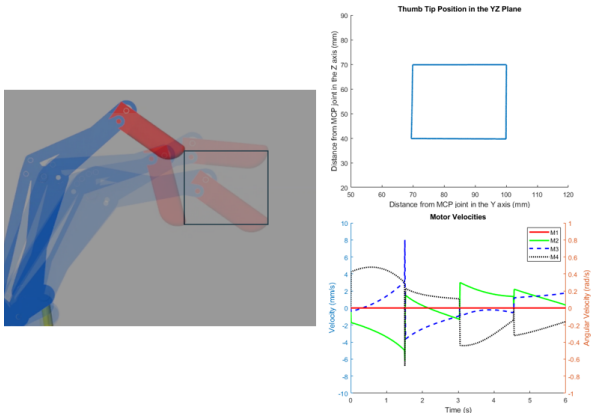

Fig. 4. Path Following in the YZ Plane

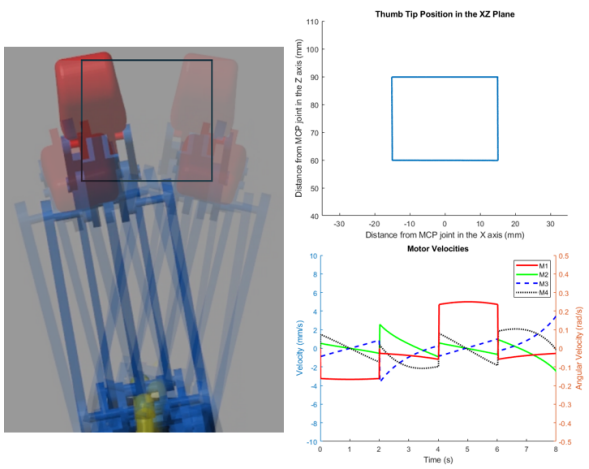

Fig. 5. Path Following in the XZ Plane

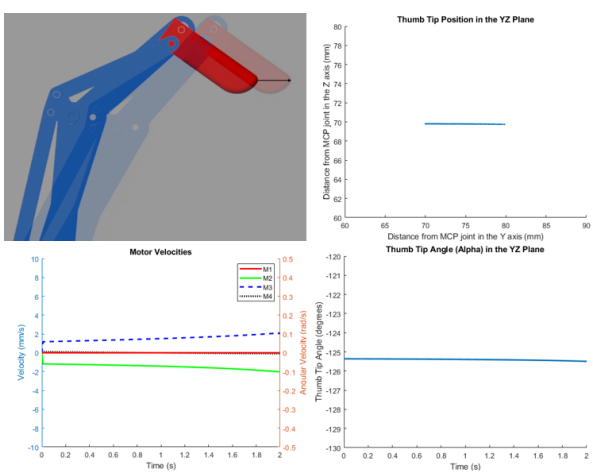

Fig. 6. Sliding Motion

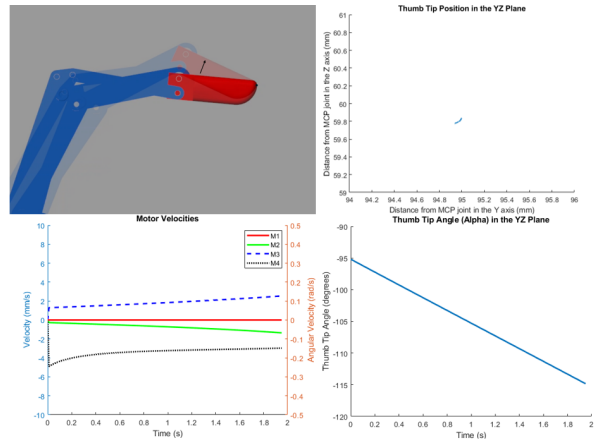

Fig. 7. Pivoting Motion

the motor velocities, and if applicable, α. A pose is defined by (x,y,z,α). Figure 4 shows the thumb following a path in the YZ plane. Starting at (0,70,70,-125°), each segment was 30 mm long and a velocity of 20 mm/s was applied to the tip. Figure 5 shows the thumb following a path in the XZ plane starting at (-15,90,90,-60°), with each segment 30 mm long and a velocity of 15 mm/s applied to the tip. In both cases, the path was followed within the error threshold stated above and completed in the expected amount of time, demonstrating both position and velocity control.

Figures 6 and 7 demonstrate the novel motions the thumb can perform. Figure 6 shows a sliding motion, where the thumb was commanded to move from (0,70,70,-125°) to (0,80,70,-125°) at 5 mm/s. Figure 7 shows a pivoting motion, where the thumb was commanded to remain in place at (0,95,60), and rotate from $\alpha = -95°$ to $\alpha = -115°$ at 10°/s. Once again the error is within our tolerances, and the motion is completed within the expected time. The code used to generate these simulations can be found at [14], and videos showing the motions, along with some preliminary five-fingered pinching simulations, can be found at [15]. The hand simulations in the video (not discussed here due to space constraints) demonstrate that the 4-DoF thumb is capable of performing pinches with each finger, achieving multiple pinch positions with the index finger, and transitioning to an open-palm configuration—despite having one fewer DoF than the anatomical thumb.

V. Summary and Future Work

We have presented the forward, inverse, and differential kinematics of a 4-DoF series-parallel robotic thumb. Building upon the work presented in [1], we demonstrate that a higher-DoF series-parallel mechanism can still be fully characterized kinematically. Moreover, we demonstrated not only Cartesian positional control, but also angular control—an essential feature for in-hand manipulation tasks that demand high dexterity and precise movement. We are currently constructing a 3-DoF series-parallel finger, as well as working to implement tactile sensors, and characterize its force output. Upon successful validation of the 3-DoF design, we plan to proceed with the construction of the 4-DoF thumb.

REFERENCES

[1] T. Zaw, D. Mahalingam, N. Baiata, A. Patankar, and N. Chakraborty, "Design and kinematic analysis of a novel series-parallel hybrid finger for robotic hands," *Journal of Mechanisms and Robotics*, vol. 17, no. 4, p. 044512, 2025, published online: November 22, 2024.

[2] S. R. Kashef, S. Amini, and A. Akbarzadeh, "Robotic hand: A review on linkage-driven finger mechanisms of prosthetic hands and evaluation of the performance criteria," *Mechanism and Machine Theory*, vol. 145, p. 103677, 2020.

[3] C. Piazza, G. Grioli, M. G. Catalano, and A. Bicchi, "A century of robotic hands," *Annual Review of Control, Robotics, and Autonomous Systems*, vol. 2, pp. 1–32, 2019.

[4] S. R. Kashef, S. Amini, and A. Akbarzadeh, "Robotic hand: A review on linkage-driven finger mechanisms of prosthetic hands and evaluation of the performance criteria," *Mechanism and Machine Theory*, vol. 145, p. 103677, 2020. [Online]. Available: https://www.sciencedirect.com/science/article/pii/S0094114X19322839

[5] L. Wu, Y. Kong, and X. Li, "Review and research issues on under-actuated finger mechanism," *Lecture Notes in Electrical Engineering*, vol. 338, pp. 171–180, 03 2015.

[6] U. Kim, D. Jung, H. Jeong, and et al., "Integrated linkage-driven dexterous anthropomorphic robotic hand," *Nature Communications*, vol. 12, p. 7177, 2021.

[7] B. Denoun, "How, where and why are researchers using the shadow dexterous hand?" 2021, published on Shadow Robot's website. [Online]. Available: https://www.shadowrobot.com

[8] AIDIN ROBOTICS, "Robotic hand," https://www.aidinrobotics.co.kr/en/robotic-hand, 2025, accessed: 2025-04-14.

[9] K. M. Lynch and F. C. Park, *Modern Robotics: Mechanics, Planning, and Control*. Cambridge, UK: Cambridge University Press, 2017. [Online]. Available: http://hades.mech.northwestern.edu/index.php/Modern_Robotics

[10] V. Nanayakkara, G. Cotugno, N. Vitzilaios, D. Venetsanos, and M. N. Sahinkaya, "The role of morphology of the thumb in anthropomorphic grasping: A review," *Frontiers in Mechanical Engineering*, vol. 3, p. 5, 2017. [Online]. Available: https://www.frontiersin.org/articles/10.3389/fmech.2017.00005/full

[11] N. Baiata, "Design and kinematic analysis of a 4-dof series-parallel hybrid thumb for robotic hands," Master's thesis, Stony Brook University, Stony Brook, NY, USA, May 2025, available at https://github.com/nickbe24/MS-Thesis-Paper.

[12] mathcentre, "Writing $a\cos(x) + b\sin(x)$ in the form $r\cos(x - \alpha)$," https://www.mathcentre.ac.uk/resources/uploaded/mc-ty-rcostheta-alpha-2009-1.pdf, 2009.

[13] D. E. Whitney, "Resolved motion rate control of manipulators and human prostheses," *IEEE Transactions on Man-Machine Systems*, vol. 10, no. 2, pp. 47–53, 1969.

[14] N. Baiata, "Github - kinematics and simulation of 4-dof series-parallel robotic thumb," 2025. [Online]. Available: https://github.com/nickbe24/Thumb

[15] ——, "Kinematics of a 4-dof series-parallel robotic thumb (supplementary video)," 2025. [Online]. Available: https://youtu.be/qrf0sRCv0kQ